ISSN 2706-655X Vol.5, Issue 12: 97-105, DOI: 10.25236/IJFET.2023.051215

Trajectory Control of Quadrotor UAV Based on Adaptive Super-twisting Sliding Mode

Yang Yang*, Wei Su

School of Information and Control Engineering, Jilin Institute of Chemical Technology, Jilin, 132000, China
**Corresponding author*

Abstract: *An adaptive super-twisting sliding mode control strategy is proposed to solve the problems of quadrotor UAV is easily disturbed by uncertainties in the environment in actual flight. Firstly, aiming at the chattering problem of traditional sliding mode control in the application process, the super-twisting sliding mode control in high-order sliding mode theory was used to weaken the chattering problem of the system. Then, aiming at the parameter adjustment problem of the controller, the adaptive control is used to automatically adjust the controller parameters to realize the trajectory tracking control, and the stability of the controller is proved based on Lyapunov theory. Finally, the simulation results show that the proposed strategy has faster response speed and higher accuracy.*

Keywords: *quadrotor UAV; adaptive; super-twisting sliding mode control; trajectory control*

1. Introduction

Thanks to the continuous development of sensor technology and computer technology, UAV technology continues to mature, and is widely used in military, agriculture, exploration and other fields[1-3]. However, due to the particularity of the flight environment of the quadrotor UAV, there are many uncertainties in the flight process, which will affect the tracking effect of the UAV on the desired trajectory. Therefore, how to improve the anti-disturbance ability and tracking accuracy of the system has become an important problem to be solved urgently in the actual flight of the quadrotor UAV. In this regard, many scholars have proposed many control schemes, such as sliding mode variable structure control[4], backstepping control[5], adaptive control[6], and cascade proportional-integral-derivative control[7]. In the above schemes, sliding mode variable structure control is widely used in the control of motors, aircraft and robots because of its simple structure, fast response speed and insensitive to disturbance.

With the wide application of industrial control system, because the output of traditional sliding mode control has chattering, the actuator of the system is difficult to execute the control output of high frequency jitter, so it is difficult to apply it to high precision control system. In order to solve this problem, scholars have proposed reaching law methods[8], boundary layer methods[9] and high-order sliding mode methods[10]. Among them, the high-order sliding mode method is widely used because of its unique design idea, which can effectively suppress chattering. Aiming at the trajectory tracking problem of the quadrotor UAV, the main work of this paper is as follows: 1) Aiming at the chattering problem of the traditional sliding mode control, the controller is designed by using the super-twisting sliding mode theory in the high-order sliding mode theory to complete the trajectory tracking control of the quadrotor UAV. 2) For the parameter adjustment of the controller, an adaptive law is designed to automatically adjust the parameters of the controller. Finally, the simulation results verify the effectiveness of the proposed strategy.

2. Modeling of quadrotor UAV

In order to describe the motion of the quadrotor UAV, the earth coordinate system and the body coordinate system are established to represent its position and attitude. Fig. 1 shows a schematic diagram of the structure of the quadrotor UAV.

ISSN 2706-655X Vol.5, Issue 12: 97-105, DOI: 10.25236/IJFET.2023.051215

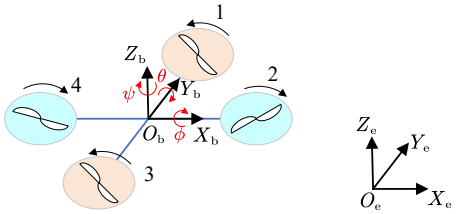

Fig. 1 Structure diagram of quadrotor UAV

The rotational speed of the four rotors increases or decreases at the same time, and the UAV moves up and down. The UAV rotates around the three axes of the body coordinate system respectively, and the UAV performs roll, pitch and yaw movements. Assume that the quadrotor UAV is a uniform and symmetric rigid body. In the earth coordinate system, starting from the kinematics of the rigid body, the Newton-Euler equation is used to describe the motion of the quadrotor UAV, and the following mathematical model can be obtained[11]:

$$\begin{cases} \ddot{x} = -\dfrac{k_f \dot{x}}{m} + \dfrac{u_x}{m} + d_x \\ \ddot{y} = -\dfrac{k_f \dot{y}}{m} + \dfrac{u_y}{m} + d_y \\ \ddot{z} = -\dfrac{k_f \dot{z}}{m} + \dfrac{u_z}{m} - g + d_z \\ \ddot{\phi} = \dfrac{1}{I_x}\left[u_2 + \dot{\theta}\dot{\psi}\left(I_y - I_z\right) - k_f \dot{\phi}\right] + d_\phi \\ \ddot{\theta} = \dfrac{1}{I_y}\left[u_3 + \dot{\phi}\dot{\psi}\left(I_z - I_x\right) - k_f \dot{\theta}\right] + d_\theta \\ \ddot{\psi} = \dfrac{1}{I_z}\left[u_4 + \dot{\phi}\dot{\theta}\left(I_x - I_y\right) - k_f \dot{\psi}\right] + d_\psi \end{cases} \tag{1}$$

High precision trajectory tracking is the main goal of controller design when the quadrotor UAV is in flight. The flight altitude is controlled by a virtual control quantity u_1 generated by the position controller, and the yaw motion is controlled by a virtual control quantity u_4 generated by the attitude controller. The desired attitude Angle ϕ_d, θ_d is calculated by the position controller based on the position virtual control quantity generated by the desired position command, and then the virtual control quantity u_2, u_3 generated by the attitude controller completes the control of the rest of the flight actions. The virtual control quantity u_1 and the desired attitude Angle ϕ_d, θ_d are shown below.

$$\begin{cases} \phi_d = \arcsin\left[\left(u_x \sin\psi_d - u_y \cos\psi_d\right)/u_1\right] \\ \theta_d = \arctan\left[\left(u_x \cos\psi_d + u_y \sin\psi_d\right)/u_z\right] \\ u_1 = \sqrt{u_x^2 + u_y^2 + u_z^2} \end{cases} \tag{2}$$

Fig.2 shows the structural block diagram of the quadrotor UAV controller. The structure contains two loops, namely the attitude control loop of the inner loop and the position control loop of the outer loop. Firstly, a position super-twisting sliding mode controller was designed for the position loop of the quadrotor UAV, and the corresponding position virtual control quantities were obtained. Then, the expected roll Angle and pitch Angle were calculated according to the position virtual control quantity. Finally, the attitude super-twisting sliding mode controller was designed to track and control the quadrotor UAV.

ISSN 2706-655X Vol.5, Issue 12: 97-105, DOI: 10.25236/IJFET.2023.051215

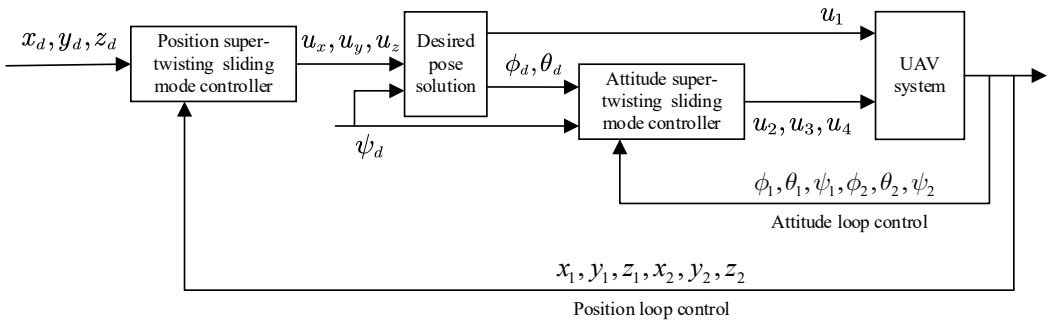

Fig. 2 Control structure block diagram

Definition The following functions are used throughout this article, defined as:

$$sig(\chi)^{\sigma} = |\chi|^{\sigma} sign(\chi) \tag{3}$$

Where $sign(\cdot)$ is sign function, $\sigma \in \mathbb{R}$ and satisfies $\sigma \geqslant 0$, $\chi \in \mathbb{R}$.

To facilitate the design, system (1) is rewritten into two subsystems: position loop and attitude loop:

$$\begin{cases} \dot{\boldsymbol{P}} = \boldsymbol{V} \\ \dot{\boldsymbol{V}} = -\dfrac{k_f}{m}\boldsymbol{V} + \dfrac{\boldsymbol{F}_p}{m} + \boldsymbol{G} + \boldsymbol{D}_p \end{cases} \tag{4}$$

$$\begin{cases} \dot{\boldsymbol{\Theta}} = \boldsymbol{\Omega} \\ \dot{\boldsymbol{\Omega}} = \boldsymbol{J}^{-1}(\boldsymbol{\tau} - \boldsymbol{\Omega} \times \boldsymbol{J}\boldsymbol{\Omega} - k_f \boldsymbol{\Omega}) + \boldsymbol{D}_a \end{cases} \tag{5}$$

3. Design of control system

3.1 Design of super-twisting sliding mode controller

Assumptions 1 Both the desired position and yaw signals are continuous and have second derivatives.

Firstly, the error between the pose of the UAV system and the desired pose and its derivative are defined as follows:

$$\begin{cases} \boldsymbol{e}_p = \boldsymbol{P} - \boldsymbol{P}_{\mathrm{d}} \\ \boldsymbol{e}_a = \boldsymbol{\Theta} - \boldsymbol{\Theta}_{\mathrm{d}} \end{cases} \tag{6}$$

$$\begin{cases} \dot{\boldsymbol{e}}_p = \boldsymbol{V} - \dot{\boldsymbol{P}}_{\mathrm{d}} \\ \dot{\boldsymbol{e}}_a = \boldsymbol{\Omega} - \dot{\boldsymbol{\Theta}}_{\mathrm{d}} \end{cases} \tag{7}$$

Based on the super-twisting sliding mode theory, the controller design is carried out in this section. In order to ensure the rapidity and stability of UAV tracking the desired trajectory, the non-singular terminal sliding mode surface[12] is selected according to the tracking error as follows:

$$s = \dot{e} + \int \left[\beta_1 sig(e)^{\alpha_1} + \beta_2 sig(\dot{e})^{\alpha_2} + \beta_3 e\right] \mathrm{d}t \tag{8}$$

Where the parameter β_1, β_2, β_3 is a positive constant, parameter α_1, α_2 is chosen such that:

ISSN 2706-655X Vol.5, Issue 12: 97-105, DOI: 10.25236/IJFET.2023.051215

$$\begin{cases} 0 < \alpha_1 < 1 \\ \alpha_2 = \dfrac{2\alpha_1}{1+\alpha_1} \end{cases} \tag{9}$$

Substituting the error equation and the system equation of the UAV, the equivalent control law can be obtained as:

$$\begin{cases} \boldsymbol{u}_{eqp} = m(\ddot{\boldsymbol{P}}_{\mathrm{d}} + \dfrac{k_f}{m}\boldsymbol{V} - \boldsymbol{G} - \boldsymbol{A}_p) \\ \boldsymbol{u}_{eqa} = \boldsymbol{J}(\ddot{\boldsymbol{\Theta}}_{\mathrm{d}} + \boldsymbol{J}^{-1}\boldsymbol{\Omega} \times \boldsymbol{J}\boldsymbol{\Omega} + \boldsymbol{J}^{-1}k_f\boldsymbol{\Omega} - \boldsymbol{A}_a) \end{cases} \tag{10}$$

Where $\boldsymbol{A}_p = [A_x \quad A_y \quad A_z]^{\mathrm{T}}$, $\boldsymbol{A}_a = [A_\phi \quad A_\theta \quad A_\psi]^{\mathrm{T}}$, $A_i = \beta_{i1} sig(e_i)^{\alpha_{i1}} + \beta_{i2} sig(\dot{e}_i)^{\alpha_{i2}} + \beta_{i3} e_i$ $\left(i = x,\ y, z, \phi, \theta, \psi\right)$. The switching control law designed using the superhelix algorithm is as follows:

$$\begin{cases} \boldsymbol{u}_{swp} = m\left[-\boldsymbol{\lambda}_{p1} sig(\boldsymbol{s}_p)^{1/2} - \boldsymbol{\lambda}_{p2}\int sign(\boldsymbol{s}_p)\,\mathrm{d}t\right] \\ \boldsymbol{u}_{swa} = \boldsymbol{J}\left[-\boldsymbol{\lambda}_{a1} sig(\boldsymbol{s}_a)^{1/2} - \boldsymbol{\lambda}_{a2}\int sign(\boldsymbol{s}_a)\,\mathrm{d}t\right] \end{cases} \tag{11}$$

Taking the above into account, the nonsingular superhelix terminal sliding mode controller based on nonsingular terminal sliding surface and superhelix switching law designed for systems (5) and (6) is shown as follows:

$$\begin{cases} \boldsymbol{u}_p = \boldsymbol{u}_{eqp} + \boldsymbol{u}_{swp} \\ \boldsymbol{u}_a = \boldsymbol{u}_{eqa} + \boldsymbol{u}_{swa} \end{cases} \tag{12}$$

3.2 Adaptive law design

Assumptions 2 The disturbance of the interfering system is continuously differentiable and satisfies $\left|\dot{d}_i\right| \leqslant \delta_i$. Where $\delta_i \left(i = x,\ y,\ z,\ \phi,\ \theta,\ \psi\right)$ is an unknown constant.

The adaptive law design method for the six degrees of freedom of the trajectory tracking control system of the quadrotor UAV is similar, and the design of the adaptive law for position x will be illustrated as an example in the following. If the interference satisfies the above assumptions, for Equations (4), (5) and (12), the adaptive law of $\lambda_{x1}, \lambda_{x2}$ in position x of Equation (12) is as follows:

$$\begin{aligned} \dot{\lambda}_{x1} &= \begin{cases} \omega_1 \sqrt{\dfrac{\gamma_1}{2}}, & s \neq 0 \\ 0 & s = 0 \end{cases} \\ \lambda_{x2} &= \chi + \frac{\varepsilon^2}{4} + \frac{\lambda_1 \varepsilon}{4} \end{aligned} \tag{13}$$

Where $\varepsilon > 4$, χ, γ_1 and ω_1 are positive constants, then s and $\dot{s}$ can converge to 0 in finite time. The control quantity at position x in Equation (12) can be obtained by substituting it into (8) and taking the derivative:

$$\dot{s}_x = -\lambda_{x1} sig(s_x)^{1/2} - \lambda_{x2}\int sign\left(s_x\right)\mathrm{d}t + d_x \tag{14}$$

Let $\dot{e}_1 = \dot{s}_x$, $\dot{e}_2 = sign\left(s_x\right) + \dot{d}_x$, Then Equation (14) can be expressed as:

ISSN 2706-655X Vol.5, Issue 12: 97-105, DOI: 10.25236/IJFET.2023.051215

$$\begin{cases} \dot{e}_1 = -\lambda_{x1} sig(e_1)^{1/2} + e_2 \\ \dot{e}_2 = -\lambda_{x2} sign(e_1) + \dot{d}_x \end{cases} \tag{15}$$

Selecting vector $\boldsymbol{\eta}^{\mathrm{T}} = [|e_1|^{1/2} sign(e_1) \quad e_2]$, consider the following Lyapunov function:

$$V(\boldsymbol{\eta}, \lambda_{x1}, \lambda_{x2}) = V_0(\boldsymbol{\eta}) + \frac{1}{2\gamma_1}(\lambda_{x1} - \lambda_{x1}^*)^2 + \frac{1}{2\gamma_2}(\lambda_{x2} - \lambda_{x2}^*)^2 \tag{16}$$

Where λ_{x1}^*, λ_{x2}^* are positive constants, $V_0(\eta) = \boldsymbol{\eta}^{\mathrm{T}} \boldsymbol{P} \boldsymbol{\eta}$, where $\boldsymbol{P} = \begin{bmatrix} \frac{4\chi + \varepsilon^2}{2} & -\frac{\varepsilon}{2} \\ -\frac{\varepsilon}{2} & 1 \end{bmatrix}$, χ, γ_1, γ_2 are positive constants, ε is any number. The derivative of a with respect to $V_0(\boldsymbol{\eta})$

$$\dot{V}_0(\boldsymbol{\eta}) = 2\lambda_{x2}\dot{e}_1 sign(e_1) + 2e_2\dot{e}_2 + \frac{1}{2}\lambda_{x1}^2 \dot{e}_1 sign(e_1) - \frac{1}{2}\lambda_{x1}|e_1|^{-1/2}\dot{e}_1 e_2 - \lambda_{x1}|e_1|^{1/2}\dot{e}_2 sign(e_1) \tag{17}$$

Substituting Equation (15), we can obtain

$$\begin{aligned} \dot{V}_0(\boldsymbol{\eta}) = &\left(-2\chi\lambda_{x1} - \frac{\varepsilon^2\lambda_{x1}}{2} + \varepsilon\lambda_{x2}\right)|e_1|^{\frac{1}{2}} + \left(2\chi + \frac{\varepsilon^2}{2} - 2\lambda_{x2} + \frac{\varepsilon\lambda_{x1}}{2}\right)e_2 sign(e_1) \\ &+2e_2\dot{d}_x - \varepsilon|e_1|^{\frac{1}{2}} sign(e_1)\dot{d}_x - \frac{\varepsilon}{2}|e_1|^{-\frac{1}{2}} e_2^2 \end{aligned} \tag{18}$$

Since $|\dot{d}_i| \leqslant \delta_i$, so $\dot{d}_x^2 \leq \delta^2$, can be obtained

$$\begin{aligned} \dot{V}_0(\boldsymbol{\eta}) \leq &\left(-2\chi\lambda_{x1} - \frac{\varepsilon^2\lambda_{x1}}{2} + \varepsilon\lambda_{x2}\right)|e_1|^{\frac{1}{2}} + \left(2\chi + \frac{\varepsilon^2}{2} - 2\lambda_{x2} + \frac{\varepsilon\lambda_{x1}}{2}\right)e_2 sign(e_1) \\ &+2e_2\dot{d}_x - \varepsilon|e_1|^{\frac{1}{2}} sign(e_1)\dot{d}_x - \frac{\varepsilon}{2}|e_1|^{-\frac{1}{2}} e_2^2 + \left(\delta^2 - \dot{d}_x^2\right)|e_1|^{\frac{1}{2}} \end{aligned} \tag{19}$$

According to the inequality condition, it can be obtained

$$\dot{V}_0(\boldsymbol{\eta}) \leqslant -\frac{1}{|e_1|^{1/2}}\boldsymbol{\eta}^{\mathrm{T}}\boldsymbol{Q}\boldsymbol{\eta} \tag{20}$$

Where

$$\boldsymbol{Q} = \begin{bmatrix} 2\chi\lambda_{x1} + \frac{\varepsilon^2\lambda_{x1}}{2} - \lambda_{x2}\varepsilon - \delta^2 - \frac{\varepsilon^2}{4} & -\chi - \frac{\varepsilon^2}{4} - \frac{\varepsilon\lambda_{x1}}{4} + \lambda_{x2} + \frac{\varepsilon}{2} \\ -\chi - \frac{\varepsilon^2}{4} - \frac{\varepsilon\lambda_{x1}}{4} + \lambda_{x2} + \frac{\varepsilon}{2} & \frac{\varepsilon}{2} - 1 \end{bmatrix} \tag{21}$$

To ensure that $\boldsymbol{Q}$ is positive definite, let

$$\lambda_{x2} = \chi + \frac{\varepsilon^2}{4} + \frac{\varepsilon\lambda_{x1}}{4} \tag{22}$$

Substituting Equation (22) into Equation (21) can be obtained

ISSN 2706-655X Vol.5, Issue 12: 97-105, DOI: 10.25236/IJFET.2023.051215

$$\boldsymbol{Q}-\frac{\varepsilon}{4}\boldsymbol{I}=\begin{bmatrix} 2\chi\lambda_{x1}+\frac{\varepsilon^2\lambda_{x1}}{2}-\chi\varepsilon-\delta^2-\frac{\varepsilon^3}{4}-\frac{\varepsilon^2}{4}-\frac{\varepsilon}{4} & \frac{\varepsilon}{2} \\ \frac{\varepsilon}{2} & \frac{\varepsilon}{4}-1 \end{bmatrix} \tag{23}$$

The condition for Q to be a positive definite matrix with the smallest eigenvalue $\lambda_{\min}(\boldsymbol{Q})>\frac{\varepsilon}{4}$ follows from the Shur complement property

$$\begin{cases} \lambda_{x1}>\dfrac{\dfrac{\varepsilon^2}{4}+\left(\varepsilon\chi+\dfrac{\varepsilon^3}{4}+\dfrac{\varepsilon^2}{4}+\dfrac{\varepsilon}{4}+\delta^2\right)\left(\dfrac{\varepsilon}{4}-1\right)}{\left(2\chi+\dfrac{\varepsilon^2}{4}\right)\left(\dfrac{\varepsilon}{4}-1\right)} \\ \varepsilon>4 \end{cases} \tag{24}$$

It can be obtained from Equation (20)

$$\dot{V}_0(\boldsymbol{\eta})\le-\frac{1}{|e_1|^{1/2}}\boldsymbol{\eta}^{\mathrm{T}}\boldsymbol{Q}\boldsymbol{\eta}\le-\frac{\varepsilon}{4|e_1|^{1/2}}\boldsymbol{\eta}^{\mathrm{T}}\boldsymbol{\eta}=-\frac{\varepsilon}{4|e_1|^{1/2}}\|\boldsymbol{\eta}\|^2 \tag{25}$$

It's going to be $\|\boldsymbol{\eta}\|_2^2=|e_1|+e_2^2$

$$\|\boldsymbol{\eta}\|_2\ge|e_1|^{\frac{1}{2}} \tag{26}$$

Therefore, Equation (25) can be written as

$$\dot{V}_0(\boldsymbol{\eta})\le-\frac{\varepsilon}{4}\|\boldsymbol{\eta}\|_2 \tag{27}$$

From $\lambda_{\min}(\boldsymbol{P})\|\boldsymbol{\eta}\|_2^2\le V_0(\boldsymbol{\eta})=\boldsymbol{\eta}^T\boldsymbol{P}\boldsymbol{\eta}\le\lambda_{\max}(\boldsymbol{P})\|\boldsymbol{\eta}\|_2^2$, it follows that

$$\left(\frac{V_0(\boldsymbol{\eta})}{\lambda_{\max}(\boldsymbol{P})}\right)^{\frac{1}{2}}\le\|\boldsymbol{\eta}\|_2 \tag{28}$$

Combining Equations (27) and (28), we obtain

$$\dot{V}_0(\boldsymbol{\eta})\le-lV_0^{\frac{1}{2}}(\boldsymbol{\eta}) \tag{29}$$

Where $l=\dfrac{\varepsilon}{4\lambda_{\max}^{\frac{1}{2}}(\boldsymbol{P})}$. The derivative with respect to $V(\boldsymbol{\eta},\lambda_{x1},\lambda_{x2})$ has

ISSN 2706-655X Vol.5, Issue 12: 97-105, DOI: 10.25236/IJFET.2023.051215

$$\begin{aligned}\dot{V}(\boldsymbol{\eta},\lambda_{x1},\lambda_{x2}) &= -lV_0^{\frac{1}{2}}(\boldsymbol{\eta})+\frac{1}{\gamma_1}(\lambda_{x1}-\lambda_{x1}^*)\dot{\lambda}_{x1}+\frac{1}{\gamma_2}(\lambda_{x2}-\lambda_{x2}^*)\dot{\lambda}_{x2}\\ &= -lV_0^{\frac{1}{2}}(\boldsymbol{\eta})-\frac{\omega_1}{\sqrt{2\gamma_1}}\left|\lambda_{x1}-\lambda_{x1}^*\right|-\frac{\omega_2}{\sqrt{2\gamma_2}}\left|\lambda_{x2}-\lambda_{x2}^*\right|\\ &+\frac{1}{\gamma_1}(\lambda_{x1}-\lambda_{x1}^*)\dot{\lambda}_{x1}++\frac{1}{\gamma_2}(\lambda_{x2}-\lambda_{x2}^*)\dot{\lambda}_{x2}\\ &+\frac{\omega_1}{\sqrt{2\gamma_1}}\left|\lambda_{x1}-\lambda_{x1}^*\right|+\frac{\omega_2}{\sqrt{2\gamma_2}}\left|\lambda_{x2}-\lambda_{x2}^*\right|\\ &\le -\min(l,\omega_1,\omega_2)(V_0(\boldsymbol{\eta})+\frac{1}{2\gamma_1}(\lambda_{x1}-\lambda_{x1}^*)^2+\frac{1}{2\gamma_2}(\lambda_{x2}-\lambda_{x2}^*)^2)^{\frac{1}{2}}\\ &+\frac{1}{\gamma_1}(\lambda_{x1}-\lambda_{x1}^*)\dot{\lambda}_{x1}++\frac{1}{\gamma_2}(\lambda_{x2}-\lambda_{x2}^*)\dot{\lambda}_{x2}\\ &+\frac{\omega_1}{\sqrt{2\gamma_1}}\left|\lambda_{x1}-\lambda_{x1}^*\right|+\frac{\omega_2}{\sqrt{2\gamma_2}}\left|\lambda_{x2}-\lambda_{x2}^*\right|\end{aligned} \tag{30}$$

It is assumed that $\lambda_{x1},\lambda_{x2}$ is all bounded when the adaptive law (13) is used. Then there exists a constant $\lambda_{x1}^*,\lambda_{x2}^*$ such that $(\lambda_{x1}-\lambda_{x1}^*)<0,(\lambda_{x2}-\lambda_{x2}^*)<0$, then Equation (30) can be written as

$$\dot{V}(\boldsymbol{\eta},\lambda_{x1},\lambda_{x2}) \le -\min(l,\omega_1,\omega_2)V(\boldsymbol{\eta},\lambda_{x1},\lambda_{x2})^{\frac{1}{2}}+\xi \tag{31}$$

Where $\xi=-\left|\lambda_{x1}-\lambda_{x1}^*\right|\left(\frac{1}{\gamma_1}\dot{\lambda}_{x1}-\frac{\omega_1}{\sqrt{2\gamma_1}}\right)-\left|\lambda_{x2}-\lambda_{x2}^*\right|\left(\frac{1}{\gamma_2}\dot{\lambda}_{x2}-\frac{\omega_2}{\sqrt{2\gamma_2}}\right)$. Let $\xi=0$, then the adaptive law of $\lambda_{x1},\lambda_{x2}$ can be obtained as

$$\begin{aligned}\dot{\lambda}_{x1} &= \omega_1\sqrt{\frac{\gamma_1}{2}}\\ \dot{\lambda}_{x2} &= \omega_2\sqrt{\frac{\gamma_2}{2}}\end{aligned} \tag{32}$$

Selecting $\varepsilon=\frac{4\omega_2}{\omega_1}\sqrt{\frac{\gamma_2}{\gamma_1}}$, equation (13) is consistent with Equation (32). When $\xi=0$, Equation (31) can be written as

$$\dot{V}(\boldsymbol{\eta},\lambda_{x1},\lambda_{x2}) \le -\min(l,\omega_1,\omega_2)V(\boldsymbol{\eta},\lambda_{x1},\lambda_{x2})^{\frac{1}{2}} \tag{33}$$

Therefore, $V(\boldsymbol{\eta},\lambda_{x1},\lambda_{x2})$ can converge to 0 in finite time, and $V_0(\boldsymbol{\eta})$ can also converge to 0 in finite time, so the sliding mode surface will converge to zero in finite time.

4. Analysis of simulation results

MATLAB/Simulink simulation platform is used in this simulation experiment, the system and controller model are built in the platform to verify the effectiveness and stability of the proposed controller. The step size in Simulink simulation is 1×10^{-3} s. The parameters of the quadrotor UAV are as follows: UAV mass $m=1\text{kg}$, wind drag coefficient $k_f=0.02$, moment of inertia on x axes $I_x=0.005445\,\text{kg/m}^2$, moment of inertia on y axes $I_y=0.005445\,\text{kg/m}^2$, moment of inertia on z axes $I_z=0.010890\,\text{kg/m}^2$, and gravitational acceleration $g=9.81\,\text{m/s}^2$. After repeated

ISSN 2706-655X Vol.5, Issue 12: 97-105, DOI: 10.25236/IJFET.2023.051215

simulation and debugging, the optimal parameters of the position loop and attitude loop controllers are selected as $\boldsymbol{\omega}_1=[5\quad 5\quad 5\quad 10\quad 10\quad 5]^{\mathrm{T}}, \boldsymbol{\gamma}_1=[2\quad 2\quad 2\quad 2\quad 2\quad 2]^{\mathrm{T}}, \boldsymbol{\chi}=[1\quad 1\quad 1\quad 1\quad 1\quad 1]^{\mathrm{T}}, \boldsymbol{\varepsilon}=[5\quad 5\quad 5\quad 5\quad 5\quad 5]^{\mathrm{T}}$, the initial value of all $\boldsymbol{\lambda}_1$ is 0.

Fig. 3 shows the trajectory tracking curve of the quadrotor UAV in 3D space. Fig. 4 shows the pose response curves.

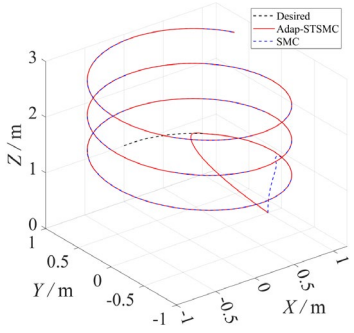

Fig. 3 Trajectory tracking curve

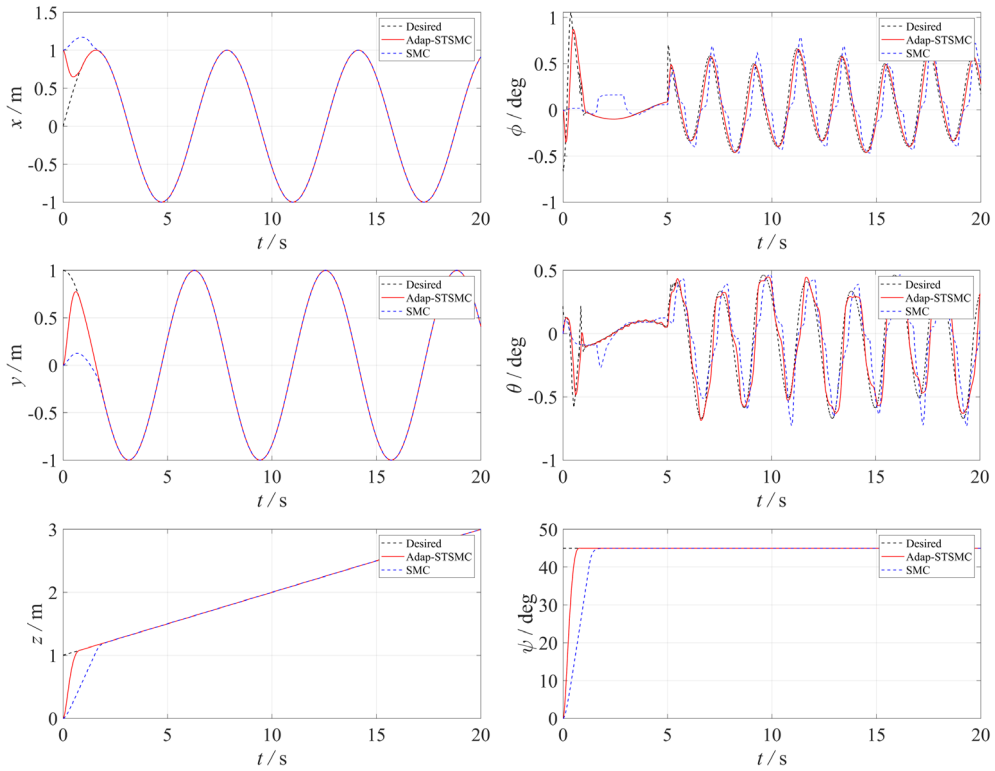

Fig. 4 Position and attitude response curve

5. Summary

In this paper, combining the super-twisting sliding mode control theory and adaptive theory, an adaptive super-twisting sliding mode control strategy is designed for the quadrotor UAV system. The simulation results show that compared with the traditional sliding mode controller, the super-twisting sliding mode control theory adopted in this paper not only has high tracking accuracy and speed for the desired trajectory, but also can significantly suppress the system chattering. In addition, the strategy adopted in this paper is more accurate for the control of attitude loop. In the future research work, we

ISSN 2706-655X Vol.5, Issue 12: 97-105, DOI: 10.25236/IJFET.2023.051215

expect to design a more effective control strategy to further weaken the chattering of the controller, and to develop a more efficient pose control scheme for the quadrotor UAV.

References

[1] Idrissi M, Salami M, Annaz F. A review of quadrotor unmanned aerial vehicles: applications, architectural design and control algorithms[J]. Journal of Intelligent & Robotic Systems, 2022, 104(2): 22.08.

[2] Wei Z, Zhu M, Zhang N, et al. UAV-assisted data collection for internet of things: A survey[J]. IEEE Internet of Things Journal, 2022, 9(17): 15460-15483.

[3] Su J, Zhu X, Li S, et al. AI meets UAVs: A survey on AI empowered UAV perception systems for precision agriculture[J]. Neurocomputing, 2023, 518: 242-270.

[4] Brahim K S, El Hajjaji A, Terki N, et al. Finite Time Adaptive SMC for UAV Trajectory Tracking under Unknown Disturbances and Actuators Constraints[J]. IEEE Access, 2023.

[5] ZHAO L, SONG X Y. Backstepping-Based Finite-Time Control for High-Order Discrete-Time Systems [J]. IEEE Transactions on Circuits and Systems II: Express Briefs, 2023, 70(6): 2127-2130.

[6] Lindqvist B, Mansouri S S, Mohammadi A A A, et al. Nonlinear MPC for Collision Avoidance and Control of UAVs with Dynamic Obstacles[J]. IEEE Robotics and Automation Letters, 2020, 5(4): 6001-6008.

[7] Song W, Li Z, Xu B, et al. Research on Improved Control Algorithm of Quadrotor UAV based on Fuzzy PID[C]//2022 IEEE International Conference on Artificial Intelligence and Computer Applications (ICAICA). IEEE, 2022: 361-365.

[8] Antonysamy R P, Lee S R, Jung S Y, et al. Performance Enhancement Using Robust Sliding Mode Approach-Based Current Control for PMVG-WECS[J]. IEEE Transactions on Industrial Electronics, 2022, 70(10): 10156-10166.

[9] Giap V N, Vu H S, Huang S C. Time-varying disturbance observer based on regulating boundary layer thickness sliding mode control for microelectromechanical systems gyroscope[J]. Measurement and Control, 2022, 55(5-6): 247-256.

[10] Cuong V N, Tuan A V, Jun H K. A Finite-Time Fault-Tolerant Control Using Non-Singular Fast Terminal Sliding Mode Control and Third-Order Sliding Mode Observer for Robotic Manipulators[J]. IEEE Access, 2021, 9: 31225 - 31235.

[11] Mahony R, Kumar V, Corke P. Multirotor aerial vehicles: Modeling, estimation, and control of quadrotor [J]. IEEE robotics & automation magazine, 2012, 19(3): 20-32.

[12] Tran X T, Kang H J. A novel adaptive finite-time control method for a class of uncertain nonlinear systems [J]. International Journal of Precision Engineering and Manufacturing, 2015, 16: 2647-2654.